Contents lists available at ScienceDirect

BBA - General Subjects

journal homepage: www.elsevier.com/locate/bbagen

Gold nanoparticles reduce tubule-interstitial injury and proteinuria in a murine model of subclinical acute kidney injury

Rodrigo A.S. Peres [a], Rodrigo P. Silva-Aguiar [a], Douglas E. Teixeira [a], Diogo B. Peruchetti [a], Sarah A.S. Alves [a], Anna Beatriz C. Leal [a], Guilherme F. Castro [a], Natalia B.S. Ribeiro [b], Fernanda V. Guimarães [b], Ana Acacia S. Pinheiro [a,c], Patrícia M.R. e Silva [b,c], Marco A. Martins [b,c], Celso Caruso-Neves [a,c,d,*]

[a] Carlos Chagas Filho Institute of Biophysics, Federal University of Rio de Janeiro, Rio de Janeiro, Brazil
[b] Laboratory of Inflammation, Oswaldo Cruz Institute, Oswaldo Cruz Foundation, Rio de Janeiro, Brazil
[c] Rio de Janeiro Innovation Network in Nanosystems for Health-NanoSAÚDE/FAPERJ, Rio de Janeiro, Brazil
[d] National Institute of Science and Technology for Regenerative Medicine, Rio de Janeiro, Brazil

ARTICLE INFO

ABSTRACT

Subclinical acute kidney injury (subAKI) is characterized by tubule-interstitial injury without significant changes in glomerular function. SubAKI is associated with the pathogenesis and progression of acute and chronic kidney diseases. Currently, therapeutic strategies to treat subAKI are limited. The use of gold nanoparticles (AuNPs) has shown promising benefits in different models of diseases. However, their possible effects on subAKI are still unknown. Here, we investigated the effects of AuNPs on a mouse model of subAKI. Animals with subAKI showed increased functional and histopathologic markers of tubular injury. There were no changes in glomerular function and structure. The animals with subAKI also presented an inflammatory profile demonstrated by activation of Th1 and Th17 cells in the renal cortex. This phenotype was associated with decreased megalin-mediated albumin endocytosis and expression of proximal tubular megalin. AuNP treatment prevented tubule-interstitial injury induced by subAKI. This effect was associated with a shift to an anti-inflammatory Th2 response. Furthermore, AuNP treatment preserved megalin-mediated albumin endocytosis in vivo and in vitro. AuNPs were not nephrotoxic in healthy mice. These results suggest that AuNPs have a protective effect in the tubule-interstitial injury observed in subAKI, highlighting a promising strategy as a future antiproteinuric treatment.

1. Introduction

Kidney disease is highly prevalent and associated with other chronic degenerative diseases and is thus a serious public health problem [1–3]. Currently, the detection of acute kidney injury (AKI) based on the Kidney Disease Improving Global Outcomes (KDIGO) guidelines is characterized by an increase in serum creatinine and/or a decrease in urine output. However, these parameters are only detected at advanced stages of the disease when treatment is less efficient [4]. The use of biomarkers of tubular injury to identify the early stages of kidney disease has created a new concept called subclinical AKI (subAKI) [5,6]. SubAKI is characterized by tubule-interstitial injury followed by changes in proximal tubular (PT) function with minimal damage to glomerular structure and function [4–6]. This process encompasses a pro-inflammatory and pro-fibrotic phenotype correlated to tubular albuminuria due to changes in megalin-mediated albumin endocytosis in PT epithelial cells (PTECs)

[7–9]. SubAKI is recognized as an emerging syndrome and a risk factor for the development of AKI and chronic kidney disease (CKD) [5,10]. Therefore, early treatment of subAKI could provide an opportunity to avoid progression of kidney injury.

Multiple forms of gold salts and their complexes have been shown to inhibit inflammation-related diseases [11]. Still, toxic renal pathological effects via direct interaction between gold ions and renal tubules limit the use of this substance for clinical application [12]. In contrast, metallic gold nanoparticles (AuNPs) appear to be safer, with low evidence of tissue damage or inflammatory changes related to acute toxicity in pre-clinical approaches [13]. These AuNPs particles may be synthesized through different chemical methods that determine their unique differences such as size, shape, and electrochemical properties making them behave differently from bulk material [14–17]. Due to the large surface-to-volume ratio of small-sized nanoparticles, AuNPs have raised interest in various biomedical areas, including biosensing, diagnostic and therapeutic [14,15]. AuNPs are particularly prone to biopharmaceutical functions because they are highly stable, bioinert, can be functionalized with therapeutic groups, and easily accumulate in the immune system [18].

Because of the well-established anti-inflammatory and antioxidant properties, AuNPs have been highlighted as a promising therapeutic strategy for several inflammatory conditions, including rheumatoid arthritis [19–21], sepsis [22] and asthma [23,24]. It is noteworthy that AuNPs are normally cleared in the kidneys, making the renal tissue a pivotal target for their action [25–27]. It has been shown that AuNPs are taken up by PTECs in a saturable mechanism, indicating a possible effect on these cells [26]. Prior studies using different models of kidney injury have shown that AuNPs ameliorate kidney damage [29–32], but the effect of these nanoparticles on renal physiological and pathological changes remains poorly understood.

In the current study, we hypothesized that AuNPs could have a beneficial effect on the development of kidney damage observed in subAKI. We report that the intraperitoneal administration of 10 nm AuNPs was not nephrotoxic for healthy mice and prevented renal damage associated with subAKI in this disease model, providing new perspectives on the use of AuNPs in the treatment of kidney injury.

2. Methods

2.1. Gold nanoparticles (AuNPs)

AuNPs were ordered from Sigma-Aldrich Brasil Ltda (#752584, São Paulo, Brazil). AuNPs were synthesized by a modified Turkevich method as previously described [33]. One hundred nM phosphate buffered saline (PBS)-stabilized AuNPs, in suspension, were further diluted in PBS before use. Polydispersity index (PDI) was lower than 0.2, whereas core size and diameter were between 8 and 12 nm and 11–25 nm, respectively, according to the manufacturer. The PBS-AuNP stability is one year in fridge according to manufacturer instructions.

2.2. Other materials and reagents

Bovine serum albumin (BSA) fraction V (#A9647), BSA conjugated to fluorescein isothiocyanate (BSA-FITC), collagenase IV, phenylmethylsulfonyl fluoride (PMSF), and protease inhibitor cocktail (no. I3786), MOPS, HEPES, EDTA, sucrose, Triton X-100, Tween 20, sodium fluoride, sodium pyrophosphate, sodium orthovanadate, sodium β-glycerophosphate, tetramethylethylenediamine (TEMED), acrylamide, bromophenol blue, 2-mercaptoethanol, periodic acid-Schiff (PAS) reagent, Sirius red, Harry's hematoxylin, Folin and Ciocalteu's phenol reagent were purchased from Sigma-Aldrich (St. Louis, MO, USA). Polyvinylidene fluoride membranes and methanol were purchased from Merck Millipore (Barueri, SP, Brazil). ECL Prime, sodium dodecyl sulfate, and Tris were purchased from GE Healthcare (Pittsburgh, PA, USA). Dulbecco's modified Eagle's medium (DMEM),

phosphate-buffered saline, fetal bovine serum (FBS), 4′,6-diamidino-2-phenylindole (DAPI), and UltraPure *N,N′*-methylenebisacrylamide (bisacrylamide) were purchased from Thermo Fisher Scientific (Waltham, MA, USA). The LLC-PK1 cell line was purchased from the ATCC (Rockville, MD, USA). A Sensiprot kit (ref. 36), creatinine kit (ref. 35–100), LDH liquiform kit (ref. 86–2/30), and γ-GT liquiform kit (ref. 105–2/50) were purchased from Labtest (Lagoa Santa, MG, Brazil). Polyclonal Lrp2/megalin (ab76969) and monoclonal albumin (ab207327) antibodies were purchased from Abcam (Cambridge, MA, USA). Anti-rabbit IgG HRP (#7074) was purchased from Cell Signal Technologies (Danvers, MA, USA). Fluorescent anti-rabbit IgG Alexa Fluor Plus 594 (A32754) was purchased from Thermo Fisher Scientific. The following antibodies were purchased from eBioscience (San Diego, CA, USA): PeCy5.5-conjugated hamster IgG1 anti-murine CD3 (145-2C11), FITC-conjugated rat IgG2b anti-mouse CD4 (clone GK1.5; 11–0041-82) and/or APC-conjugated rat IgG1 anti-murine CD25 (PC61.5; 17–0251-82), PE-conjugated rat IgG1 anti-murine IFN-γ (XMG1.2), PE-conjugated rat IgG2b anti-murine IL-4 (BVD4-1D11), and PE-conjugated rat IgG1 anti-murine IL-17 (TC11-18H10).

2.3. Animals

Male C57BL/6 mice (8–10 weeks old), weighing 18–24 g, were used in all experiments. These mice were obtained from the Institute of Science and Technology in Biomodels (ICTB) of the Oswaldo Cruz Foundation (FIOCRUZ), Rio de Janeiro, Brazil. All mice were housed, bred, and maintained in the animal care facility at the Federal University of Rio de Janeiro. The animals were accommodated in an air-conditioned environment (22 °C–24 °C) in a regular 12-h light/dark cycle with water and standard chow ad libitum. All procedures involving the handling of animals were conducted in accordance with the National Institutes of Health (NIH) Guide for the Care and Use of Laboratory Animals and were approved by the Ethics Committee of the Oswaldo Cruz Institute (CEUA/IOC number 001/2019).

2.4. Subclinical AKI animal model and AuNP treatment

The subAKI model was developed as described previously [7–9,34,35]. Briefly, mice were randomly divided into 4 experimental groups: (1) control, mice received an IP injection of saline (used as vehicle); (2) AuNP, mice received an IP injection of an AuNP suspension (10 μg/kg/day); (3) subAKI, mice received an IP injection of BSA (10 g/kg/day); (4) subAKI+AuNP, mice received simultaneous IP injections of AuNP (10 μg/kg/day) and BSA (10 g/kg/day) for 7 consecutive days. Twenty-four hours before the end of the experiment, all mice were kept in metabolic cages for 24 h urine collection. At the end of day 7, the animals were euthanized using a mixture of ketamine (240 mg/kg) and xylazine (15 mg/kg), followed by cardiac puncture for blood collection. The kidneys were perfused with heparinized saline and 4% paraformaldehyde using a peristaltic pump and extracted for further analysis: (1) histology; (2) immunofluorescence; (3) in vivo albumin endocytosis; (4) immune cell infiltration.

2.5. Analysis of renal function

Analysis of renal function was performed according to previously published studies [7–9,33]. In brief, 24 h urine samples were quantified to determine urinary output and urinary flow (mL/min). Then, the samples were clarified by 5 cycles of centrifugation (10,000 ×g for 10 min) to remove urine sediments. The urinary levels of creatinine, proteinuria, γ-glutamyl transferase (γ-GT), and lactate dehydrogenase (LDH) were measured. Plasma was obtained by centrifuging whole blood (2500 ×g for 5 min). The plasma creatinine and blood urea nitrogen (BUN) levels were analyzed. All the parameters were analyzed using commercial kits from Labtest (Lagoa Santa, MG, Brazil). The results were used to calculate the urinary protein to creatinine ratio

(UPCr) and the estimated glomerular filtration rate (eGFR), which relies on the renal clearance of creatinine (mL/min).

2.6. Histologic analysis

Histologic analysis was performed as described previously [7–9,36]. In brief, perfused kidneys were fixed in 10% formalin buffer and embedded in paraffin. Then, 5- and 8-μm-thick slices of the kidneys were stained with PAS and Picrosirius red, respectively. All images of the renal cortex were acquired using a Nikon 80i eclipse microscope (Nikon, Japan). Quantification of the images was done in a blinded analysis using Image-Pro Plus Software (Media Cybernetics, Rockville, MD, USA). The cortical tubule-interstitial area was determined by directly measuring the area between cortical tubules, expressed as a percentage of the total area. Collagen deposition was analyzed by measuring the intensity of red fibers in selected hot spot areas, expressed as the fold change. Glomerular area, expressed in μm^2, corresponds to the area delimited by the outer side of Bowman's capsule.

2.7. Immunofluorescence and confocal microscopy

Analyses of immunofluorescence were performed following previous studies [8,9,36]. Briefly, immunofluorescence analysis of megalin was performed using 5-μm kidney slices prepared as described in Section 2.5. Anti-rabbit megalin antibody (1:100) was incubated overnight at 4 °C. Fluorescent anti-rabbit IgG Alexa Fluor 594 (1:200) was incubated for 1 h at room temperature. The cell nuclei were stained with DAPI for 5 min at room temperature. The tissue slices were mounted with anti-fade mounting medium. Image visualization and acquisition were performed by confocal microscopy (Leica TCS SP8, Leica, Wetzlar, Germany). The images were then analyzed using FIJI software version 2.1.0 (NIH, Bethesda, MD, USA). The Interactive 3D Surface Plot plugin v2.4.1 was used for 3D projection. The intensity of the megalin signals was highlighted by applying a colorized Thermal Look-Up Table on individual PT segments selected as regions of interest. The apical to basolateral distribution of megalin was analyzed by generating a plot profile of the signal intensities from the luminal to the basolateral side of individual PT cells by drawing a straight segment along each cell [37]. The megalin expression in the brush border was quantified by calculating the area under the curve of the plot profile peaks.

2.8. Albumin-FITC uptake in vivo

Albumin-FITC uptake in vivo was measured in the renal cortex as previously reported [7–9,36]. Briefly, mice received an intravenous injection of BSA-FITC (5 μg/g body weight) through the tail vein. After 15 min, the kidneys were extracted. The renal cortex was separated and homogenized in ice-cold Ringer solution (20 mM HEPES–Tris [pH 7.4], 5 mM D(+)-glucose, 2.7 mM KCl, 140 mM NaCl, 1 mM MgCl₂, 1.8 mM CaCl₂) containing 1 mM PMSF and 1× protease inhibitor cocktail. Samples were clarified by centrifugation (10,000 ×g for 10 min). The cortex-associated fluorescence was measured in the supernatant using a SpectraMax M2 microplate reader (Molecular Devices, San Jose, CA, USA). The specific albumin-FITC uptake was further normalized by the total protein concentration of each sample. Data are expressed as arbitrary units.

2.9. Immune cell infiltration

Immune cell infiltration in the kidneys was assessed as reported previously [34,38]. Briefly, the kidneys were cut into pieces and enzymatically digested in a solution containing 0.1% collagenase for 60 min at 37 °C. The digested homogenate was filtered through 100-μm filters to isolate immune cells. Analysis of surface markers was performed by incubating the cells with the appropriate concentrations of the following antibodies: PeCy5.5-conjugated hamster IgG1 anti-murine CD3 (145-

2C11), FITC-conjugated rat IgG2b anti-mouse CD4 (clone GK1.5; 11–0041-82), and/or APC-conjugated rat IgG1 anti-murine CD25 (PC61.5; 17–0251-82) purchased from eBioscience (San Diego, CA, USA). To determine the specific cell phenotypes, the cells were fixed and permeabilized with Citofix/Citoperm (BD Pharmingen, San Diego, CA, USA) and incubated with the following antibodies: PE-conjugated rat IgG1 anti-murine IFN-γ (XMG1.2), PE-conjugated rat IgG1 anti-murine IL-17 (TC11-18H10), and PE-conjugated rat IgG2b anti-murine IL-4 (BVD4-1D11), or isotype-matched antibodies purchased from eBioscience. After incubation, the cells were analyzed in a BD FACSCalibur cytofluorometer (BD Biosciences) using CellQuest software.

2.10. Cell culture

LLC-PK1 cells, a well-established porcine PTEC line [39–41], were obtained from ATCC (Rockville, MD, USA). The cells were cultured in low-glucose DMEM supplemented with 10% FBS and 1% penicillin/streptomycin at 37 °C in humidified air containing 5% CO_2, as described previously [8,9,36]. Cells were seeded in 24-well plates and grown for 2 days until reaching 85%–90% confluence. Then, the cells were serum starved overnight and treated with AuNPs (1 μg/mL) and albumin (20 mg/mL) alone or in combination to assess albumin endocytosis in vitro, as shown in the figure legends.

2.11. Albumin endocytosis in vitro

Albumin endocytosis in vitro was performed according to previous studies [9,42,43]. After the indicated treatments, the cells were washed 3 times and incubated with Ringer solution (20 mM HEPES–Tris [pH 7.4], 5 mM D(+)-glucose, 2.7 mM KCl, 140 mM NaCl, 1 mM MgCl₂, 1.8 mM CaCl₂) containing 100 μg/mL BSA-FITC at 37 °C for 30 min. After incubation, the cells were kept on ice, and unbound BSA-FITC was removed by washing the cells 10 times with ice-cold Ringer solution. Then, the cells were lysed with a buffered detergent solution containing 20 mM MOPS (pH 7.4) and 0.1% Triton X-100. The homogenate was collected to measure the cell-associated fluorescence using a SpectraMax M2 microplate reader (Molecular Devices). The specific fluorescence of endocytosed BSA-FITC was obtained by subtracting non-specific fluorescence of BSA-FITC uptake determined on cells co-incubated with unlabeled BSA (100 mg/mL). The specific cell-associated fluorescence was further normalized to the total protein concentration of each sample. Data are expressed as arbitrary units.

2.12. Statistical analysis

All results are presented as medians (interquartile range). The Shapiro-Wilk test was used to evaluate normal data distribution. To compare differences between groups, one-way analysis of variance was used followed by Tukey's post-test. $P < 0.05$ was considered statistically significant. GraphPad Prism 8 (version 8, GraphPad Software, San Diego, CA, USA) was used for the statistical analysis.

3. Results

3.1. SubAKI and AuNP-treated animals present no change in glomerular function and morphology

Four experimental groups, described in Section 2, were used to test the possible effect of AuNPs on the development of subAKI: (1) control; (2) AuNP; (3) subAKI; (4) subAKI+AuNP. Body weight, food intake, water intake, urinary flow, and urinary creatinine were not changed among the groups (Table 1). Markers of glomerular function such as plasma creatinine, BUN, and eGFR, as well as glomerular area assessed in PAS-stained kidney slices, were not changed among the groups (Fig. 1A–E). These results show that glomerular function and structure were unchanged in the AuNP and subAKI groups.

Table 1
Functional parameters (Mean ± SD).

Parameters	Control (n = 10)	AuNP (n = 10)	subAKI (n = 10)	subAKI + AuNP (n = 10)
Body weight (g)	18.48 ± 1.18	17.88 ± 1.94	18.30 ± 1.69	18.20 ± 3.14
Food intake (g/24 h)	4.34 ± 1.12	4.05 ± 1.14	3.91 ± 0.32	3.22 ± 1.13
Water intake (g/ 24 h)	8.75 ± 4.92	8.60 ± 3.84	10.00 ± 2.00	6.00 ± 2.82
Urinary flow (μL/ min)	0.95 ± 0.33	0.85 ± 0.12	0.87 ± 0.23	0.80 ± 0.17
Urinary creatinine (mg/dL)	31.50 ± 10.58	41.63 ± 15.47	38.23 ± 13.18	36.35 ± 15.85

3.2. Tubule-interstitial injury observed in subAKI is ameliorated by AuNPs

Specific markers of PT injury, including urinary γ-GT and LDH activities, were analyzed. The subAKI group presented a higher activity of urinary γ-GT and LDH compared with the control group (Fig. 2A,B). Furthermore, 24 h proteinuria and the UPCr, as well as albuminuria, measured by immunoblotting, were also increased in the subAKI group compared with the control group (Fig. 2C–I). These effects were avoided when the animals were treated simultaneously with AuNPs (subAKI+AuNP group).

In agreement with the observed functional parameters, animals in the subAKI group presented increased cortical interstitial space area and collagen deposition (Fig. 3A–D). Simultaneous treatment with AuNPs (subAKI+AuNP group) avoided the development of tubule-interstitial injury. Treatment of the animals with AuNPs alone (AuNP group) did not change the parameters shown in Table 1 and Figs. 2 and 3. These observations indicate that the treatment with AuNPs did not promote toxic effects.

CD4+ T cells have a role in the development of subAKI, therefore we evaluated the possible modulation of these cells by AuNPs using fluorescence-activated cell sorting analysis (Fig. 4A). The increase in the activation markers (CD3+ CD4+ CD25+) observed in the subAKI group was avoided when animals were treated simultaneously with AuNP (subAKI+AuNP group) (Fig. 4B,C). Activated CD4+ T cells were not detected in the AuNP group. Moreover, activated CD4+ T cells in the subAKI group followed Th1 and Th17 phenotype differentiation, characterized by an increase in the production of interferon γ (IFN-γ) and IL-17, respectively (Fig. 4D–I). On the other hand, the IL-4-producing Th2 phenotype was not changed. Simultaneous AuNP treatment (subAKI+AuNP group) abolished CD4+ T cell differentiation to the pro-inflammatory profiles. Furthermore, the Th2 profile was increased in the AuNP and subAKI+AuNP groups. These results demonstrate that AuNP treatment ameliorates tubule-interstitial injury observed in an animal model of subAKI, which is correlated with a switch from a pro-inflammatory to an anti-inflammatory phenotype.

3.3. AuNP treatment prevents reduction of albumin-FITC uptake and megalin expression

SubAKI is characterized by tubular albuminuria due to changes in megalin-mediated endocytosis in PTECs [7–9]. In vivo albumin-FITC uptake in the renal cortex was analyzed to evaluate the possible modification of this mechanism in the different groups. The subAKI group showed reduced uptake of albumin-FITC compared with the control group (Fig. 5A). This decrease in albumin-FITC uptake was not observed when the animals were treated simultaneously with AuNPs (subAKI+AuNP group). Albumin uptake in vivo was not changed in the AuNP group compared with the control group.

We then wanted to determine if the effect of AuNPs on albumin endocytosis could occur directly in PTECs. To address this issue, albumin uptake was measured in LLC-PK1 cells, a model of PTECs [40,41]. To mimic the subAKI condition, LLC-PK1 cells were treated overnight with a higher albumin concentration (20 mg/mL) [44–46]. Albumin uptake was decreased under these conditions (Fig. 5B). On the other hand, the simultaneous treatment of LLC-PK1 cells with 1 μg/mL AuNP avoided the decrease in albumin-FITC uptake. The addition of AuNP alone did not change albumin-FITC uptake. These results are similar to those observed in the animal model indicating that AuNP could have a direct effect on albumin endocytosis in PTECs.
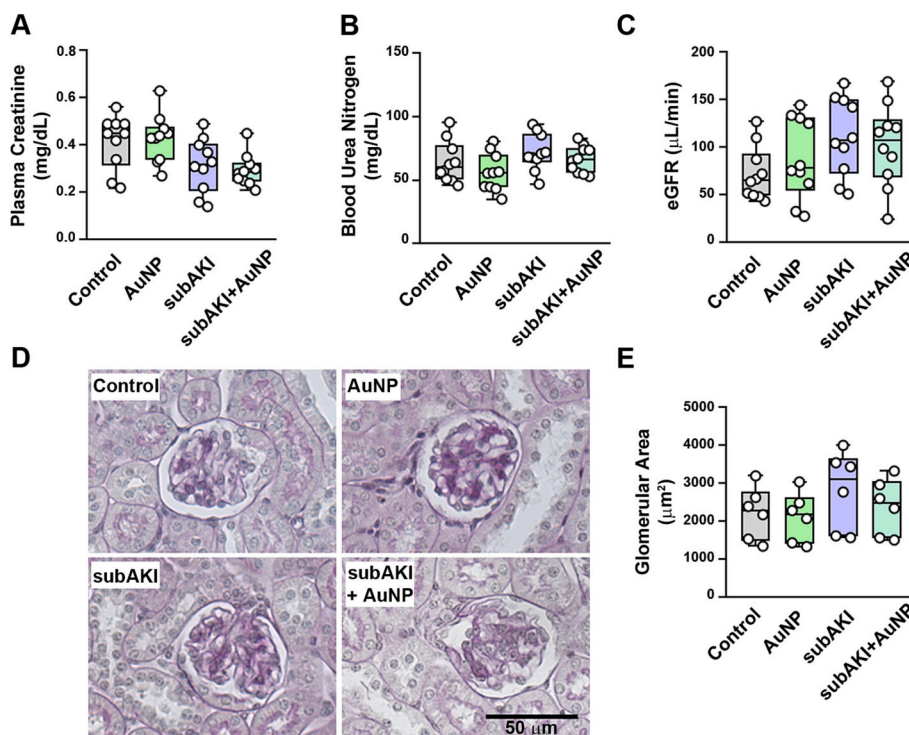
Fig. 1. AuNP treatment does not change glomerular function and structure. Functional and structural analyses were performed on each experimental group as described in Section 2. (A) Plasma creatinine (n = 10); (B) blood urea nitrogen (BUN) (n = 10); (C) estimated glomerular filtration rate (eGFR) measured by creatinine clearance (n = 10). (D) Representative micrographs of cortical glomerulus in PAS-stained kidney sections. Scale bar, 50 μm. (E) Quantitative analysis of glomerular area (μm²) (n = 6). Data are presented as medians (interquartile range).
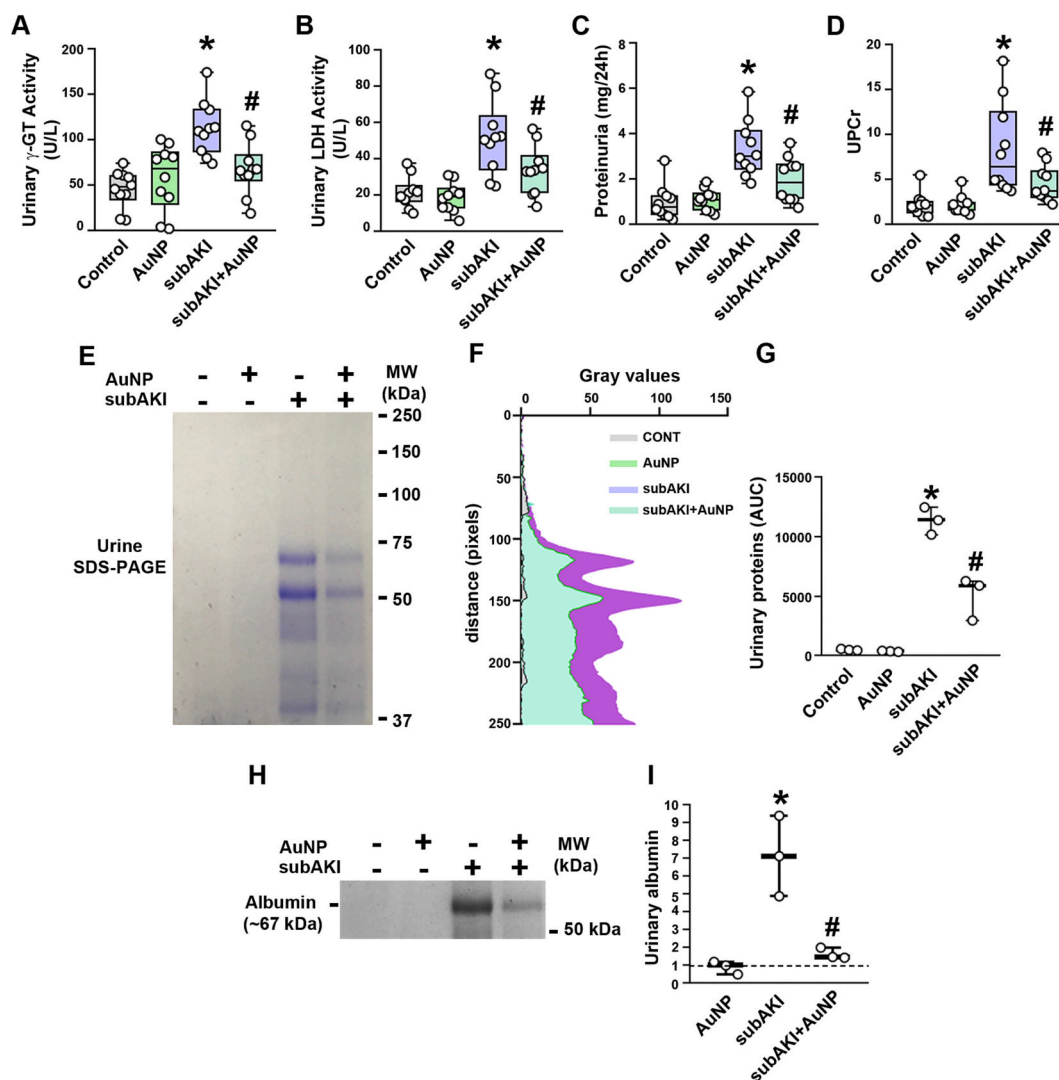
Fig. 2. AuNP treatment ameliorates proximal tubule injury and proteinuria observed in an animal model of subAKI. (A) Urinary γ-glutamyl transferase (γ-GT) activity (n = 10); (B) urinary lactate dehydrogenase (LDH) activity (n = 10); (C) 24-h proteinuria (n = 10); (D) urinary protein creatinine ratio (UPCr) (n = 10); (E) assessment of urinary proteins by SDS-PAGE stained with Coomassie blue; representative image of 3 independent experiments; (F) plot profile analysis of urinary protein from SDS-PAGE; (G) urinary protein expression quantified by the area under the curve (AUC) of representative plot profiles from each group; (H) representative immunoblotting image of urinary albumin from 3 independent experiments; (I) densitometry of urinary albumin immunoblotting (*n* = 3). Data are presented as medians (interquartile range). *$P < 0.05$ in relation to the control group. #$P < 0.05$ in relation to the subAKI group. (For interpretation of the references to colour in this figure legend, the reader is referred to the web version of this article.)

To obtain additional insights into the molecular mechanism, megalin expression in an animal model was analyzed by immunofluorescence followed by confocal microscopy analysis. Total PT megalin expression was reduced in the subAKI group compared with the control group (Fig. 5C,D). Simultaneous treatment with AuNP avoided this inhibitory effect. Megalin function depends on its localization on the apical brush border of PTECs [47], therefore we analyzed the apical to basolateral distribution of megalin signal intensity in individual PT cells. In accordance with total PT megalin expression, brush border megalin expression was decreased in the subAKI group compared with the control group (Fig. 5E–G). Similarly, the ratio between brush border and total megalin expression was not changed, indicating that its cellular traffic was not modified (Fig. 5E–H). The inhibitory effect was not observed in the subAKI+AuNP group. Both total PT and brush border megalin expression were not changed in the AuNP group. All these results correlate with the increase in 24 h proteinuria, UPCr, and albuminuria (Fig. 2C–F).

4. Discussion

Early diagnosis and management of kidney disease remains a challenge for clinicians and nephrologists due to the silent nature of renal diseases and the use of inaccurate diagnostic markers, such as plasma creatinine levels [48,49]. The detection of early tubule-interstitial injury through specific biomarkers in subAKI provides an opportunity for early therapeutic intervention. Our results provide new perspectives on the use of AuNPs in the treatment of kidney injury at the early stage, halting its progression to AKI and CKD.

One of the main concerns about using nanoparticles such as AuNPs is the possible toxic effects [50,51]. The side effects of naked AuNPs might be related to different treatment protocols, including dosage, route of administration, treatment duration, and characteristics of the nanoparticles [52–56]. Isoda et al. [57] showed that intravenous infusion of 10–100 nm naked AuNPs (4 mg/kg) in male BALB/c mice did not present nephrotoxicity, measured by serum creatinine and BUN, 24 h after injection. Here, we also demonstrated that IP injection of 10-nm naked AuNPs (10 μg/kg) in male C57BL/6 mice did not lead to nephrotoxicity
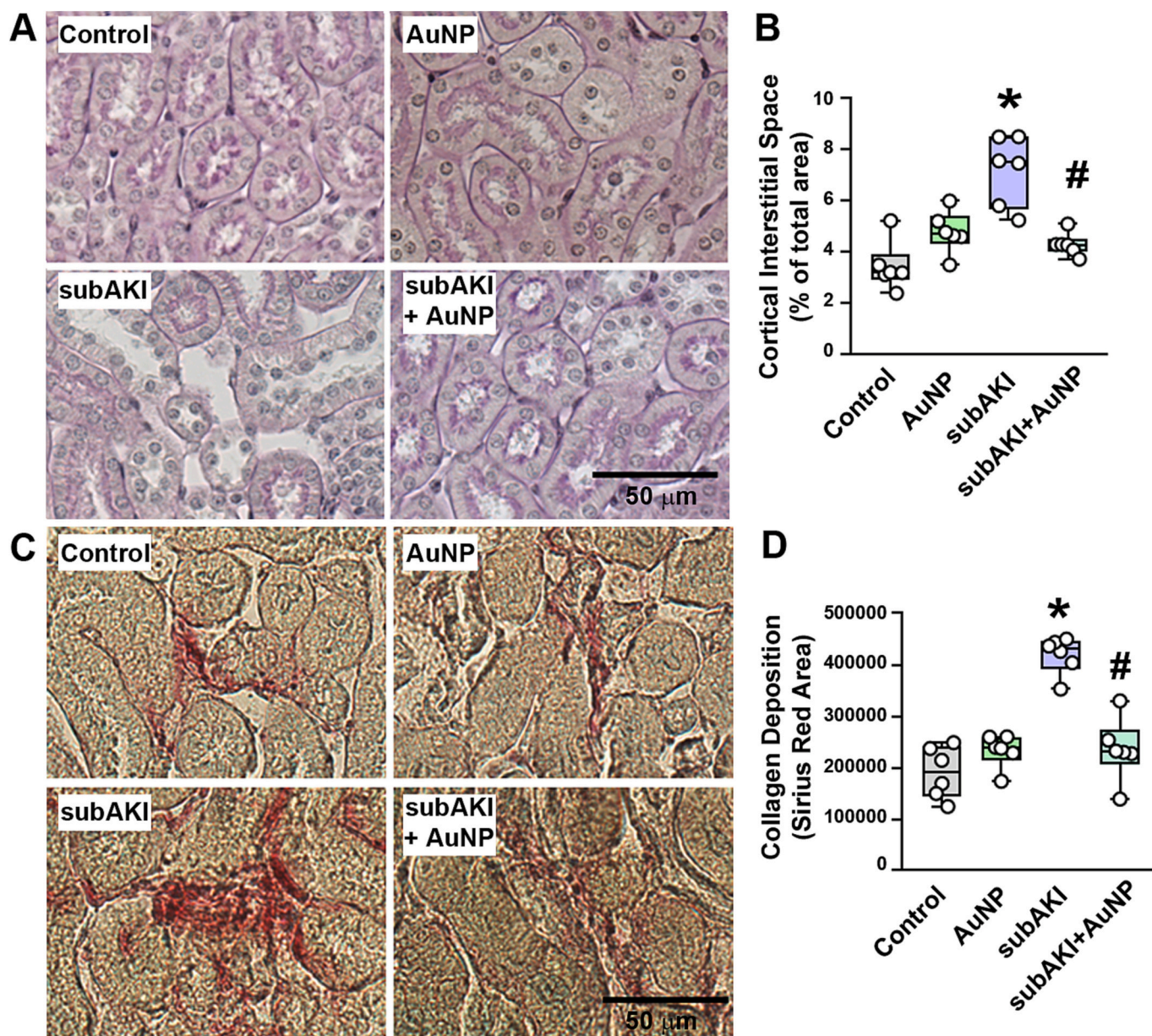
Fig. 3. AuNP treatment prevents the increase in tubule-interstitial space and collagen deposition in an animal model of subAKI. (A) Representative micrographs of cortical tubule-interstitial area in PAS-stained kidney sections. (B) Quantitative analysis of the cortical interstitial space area (n = 6). (C) Representative micrographs of hotspots of collagen deposition in kidney sections stained with Picrosirius red. Scale bar, 50 μm. (D) Quantitative analysis of collagen deposition (n = 6). Data are presented as medians (interquartile range). *P < 0.05 in relation to the control group. #P < 0.05 in relation to the subAKI group. (For interpretation of the references to colour in this figure legend, the reader is referred to the web version of this article.)

up to 1 week after the injection. Nephrotoxicity was assessed by glomerular and tubular structural and functional parameters, including proteinuria and albuminuria. On the other hand, Al-Harbi et al. [58] showed IP administration of a single dose of 5-nm naked AuNPs (25 μg/kg) to rats caused mild shrinkage in Bowman's space 24 h after the injection. The authors did not observe changes in the immune profile as in our results. The differences observed could be due to the time of analysis after injection and/or the animal species used.

One important question regards to interaction of AuNP with blood/plasma/serum. We did not assess blood compatibility directly in the present work. However, this approach has been performed previously by other authors. He et al. [59] analyzed the effect of 13-nm AuNPs on human blood by incubating whole blood with AuNPs. The authors observed plasma distribution, as well as uptake by platelets, leucocytes, and erythrocytes. There were no detectable changes in hemolytic and

deformability parameters of erythrocytes, even with the highest dose used (100 mg/mL). Furthermore, Aseichev et al. [60] observed that a higher concentration of AuNP (20 μM) did not cause erythrocyte hemolysis after incubation for 4 h. Here, we used AuNP at a lower concentration (50 nmol/kg). These data provide evidence of blood compatibility and no toxic effects of AuNPs in both in vitro and in vivo models [59,60].

Smaller AuNPs (≤10 nm) are filtered through the glomerulus and excreted into the urine, whereas the larger particles are retained by the glomerular filtration membrane [25–27]. AuNPs can interact with PTECs and be retained by these cells with huge absorptive capacity [28]. Our results showed that AuNPs could directly modulate albumin uptake in LLC-PK1 cells, a model of PTECs. Therefore, targeting specific nephron segments and cell types with AuNPs of different sizes might be a possibility for the treatment of different kidney diseases, such as
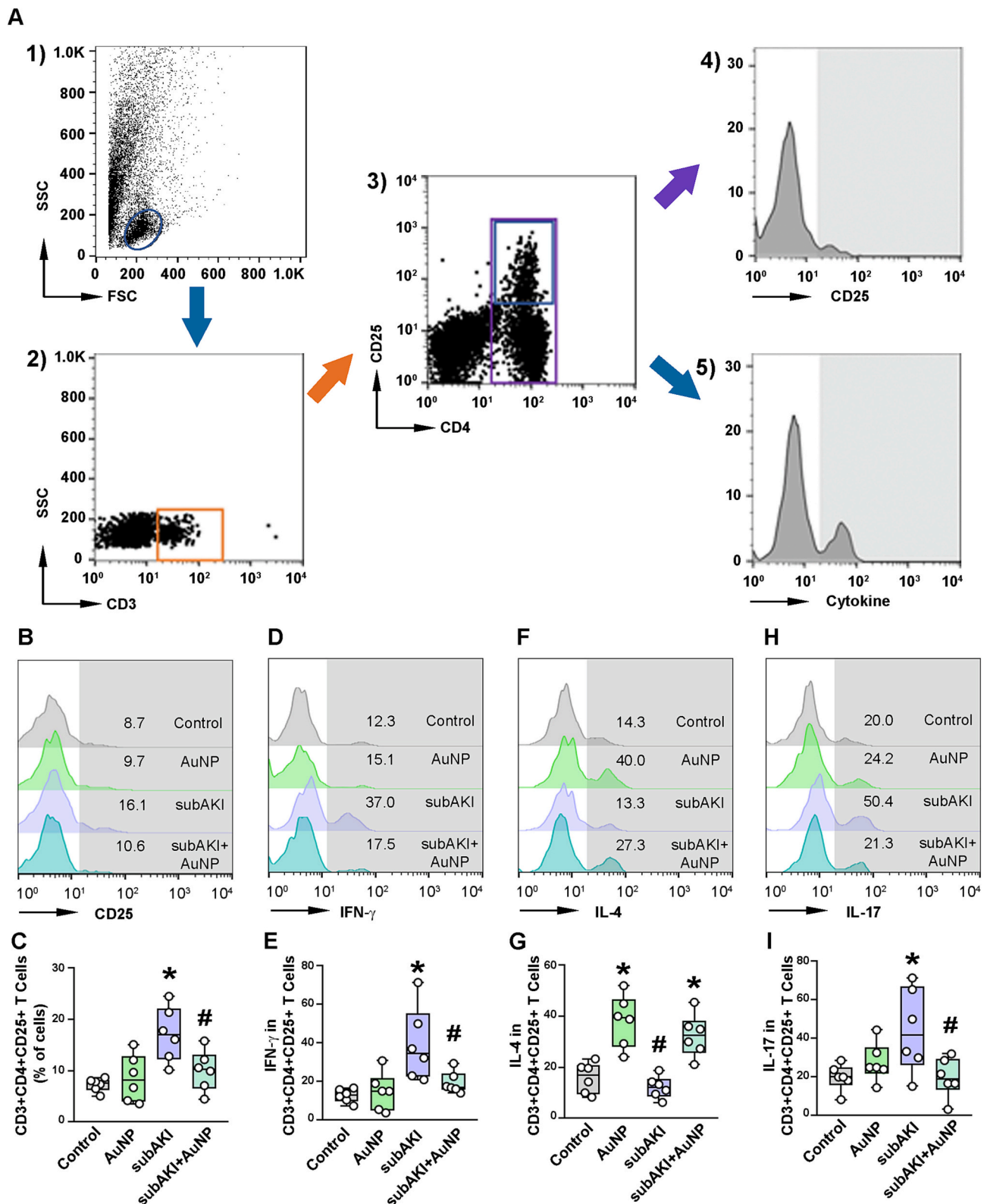
Fig. 4. Pro-inflammatory profile in an animal model of subAKI treated or not with AuNPs. (A) Gate strategy used to analyze renal T cells. Step 1, the lymphocyte population was selected by ungated forward and side scatter plot (FSC × SSC). Step 2, CD3 staining was used to detect the T cell population in lymphocyte cells. Step3, CD4 (purple gate) CD25 (blue gate) staining was used to detect activated CD4+ T cells in the CD3 + -gated population. Step 4, histogram representation of CD4 + CD25+ T cells. Step 5, cytokine analysis in CD4 + CD25+ T cells. (B) Representative histograms of renal CD3 + CD4 + CD25+ T cells. (C) Quantitative analysis of renal CD3 + CD4 + CD25+ T cells (n = 6); (D, F, H) Representative histograms showing the proportion of specific CD3 + CD4 + CD25+ T cell subsets, including Th1 (IFN-γ), Th2 (IL-4), and Th17 (IL-17) phenotypes, respectively. (E, G, I) Quantitative analysis of CD3 + CD4 + CD25+ T cell specific subsets (n = 6). The gray areas in the histograms represent the population analyzed. The values on each histogram represent the percentage of cells. Data are presented as medians (interquartile range). *P < 0.05 in relation to the control group. #P < 0.05 in relation to the subAKI group. (For interpretation of the references to colour in this figure legend, the reader is referred to the web version of this article.)
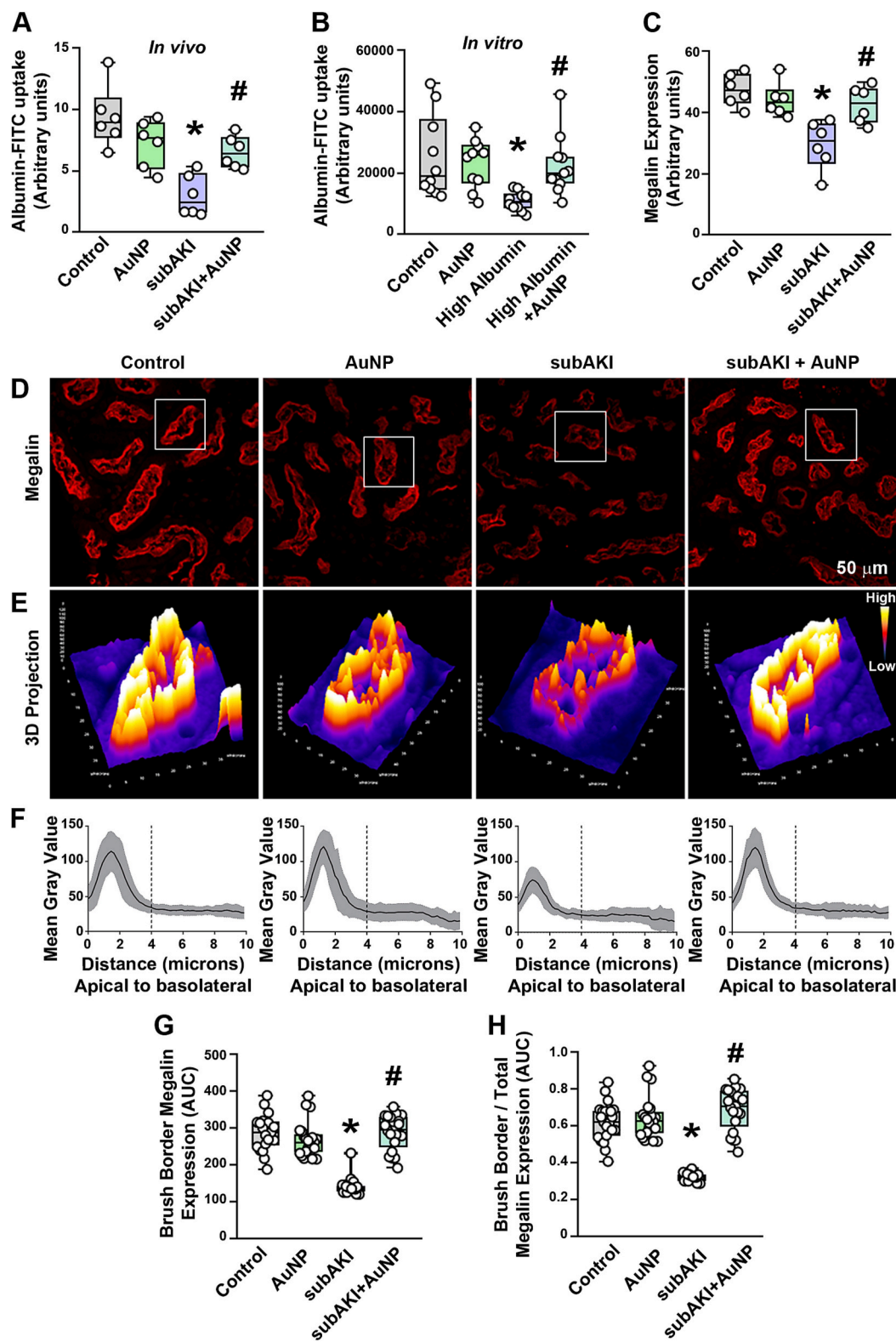
Fig. 5. AuNP modulates megalin-mediated proximal tubule albumin uptake. (A) Cortical albumin-FITC uptake in vivo in different experimental groups (n = 6). (B) Albumin-FITC uptake in LLC-PK1 cells treated with AuNPs (1.0 μg/mL) and/or high albumin (20 mg/mL) for 16 h (n = 10). (C) Representative confocal microscopy images of megalin expression in cortical PTECs assessed by immunofluorescence. (D) Quantification of total megalin expression in PTECs (n = 6). (E) Representative 3D projection of tubular megalin expression. (F) Plot profile analysis of apical to basolateral membrane distribution of megalin in the PTECs was determined as described in Section 2 (n = 3). Dashed lines depict the expected height of the PT brush border (~4 μm). (G) Brush border megalin expression quantified by the area under the curve (AUC) of representative plot profile peaks from each group (n = 3, symbols represent the number of different plot profile peaks analyzed from different cells). (H) Ratio between brush border and total megalin expression (n = 3, symbols represent the number of plot profile curves analyzed from different cells). Data are presented as medians (interquartile range). *P < 0.05 in relation to the control group. #P < 0.05 in relation to the subAKI group.

glomerulopathies and tubulopathies [30,31]. Some studies have reported beneficial effects of nanoparticles on animal models of kidney disease [27,30,31].

Here, we showed that IP treatment with naked AuNPs avoided the development of tubule-interstitial injury observed in the subAKI animal model. It has been shown that subAKI presents an intense inflammatory response associated with increases in pro-inflammatory cytokines, chemokines, and activation of immune cells in renal cortical segments [7,8]. Our results in the present work confirm the inflammatory profile of subAKI. Naked AuNPs modulate immune responses due to their interaction with immune cells [61,62]. It has been shown that AuNPs induce the secretion of anti-inflammatory cytokines to the detriment of pro-inflammatory cytokines in LPS-stimulated dendritic cells [63,64]. Rizwan et al. [65] demonstrated that AuNPs reduced the pro-inflammatory response of macrophages induced by high glucose. Our results showed that the treatment with naked AuNPs switched the pro-inflammatory profile observed in subAKI to an anti-inflammatory profile measured by reduction the in Th1 (IFN-γ) and Th17 (IL-17) responses and an increase in the Th2 (IL-4) response.

Usually, the effects of IL-4 are associated with anti-inflammatory and pro-resolutive action [66]. In agreement with this view, it was observed previously that IL-4 has a protective effect on the development of tubule-interstitial injury in an animal model of subAKI [8]. This effect was correlated with modulation of the pro-inflammatory response mediated by IL-6 and IL-17. On the other hand, it has been proposed that IL-4 is implicated in enhancing the pro-inflammatory response in asthma due to the increase in inflammatory cell infiltration [67,68]. AuNP treatment was found to reduce the IL-4 level in murine models of atopic asthma, shifting the pro-inflammatory response to anti-inflammatory due to reduced inflammatory cell infiltration [23]. Therefore, the action of AuNPs in both diseases involves a shift in the overall response from pro-inflammatory to anti-inflammatory rather than a specific effect on the production of a particular cytokine.

In agreement with our results, Alomari et al. [32] reported that 50-nm AuNPs could improve renal function in rats with diabetic nephropathy. These effects were associated with the reduced renal expression of pro-fibrotic markers (TGF-β, fibronectin, collagen IV) and TNF-α. In addition, it has been shown that treatment with 20-nm naked AuNPs reduced tubular injury in a model of schistosomiasis-induced nephrotoxicity [30]. The authors observed an improvement in tubule-interstitial injury associated with reduced expression of KIM-1 and NGAL, markers of tubular injury, as well as TFG-β and MCP-1. In agreement, we also showed a decrease in collagen deposition associated with a decrease in urinary γ-GT and LDH activities in the subAKI group when the animals were treated with naked AuNPs.

Besides the immune-mediated effects of AuNPs, direct interaction of these particles with PTECs is another attractive hypothesis to explain the beneficial effects of AuNPs in subAKI. In the present study, we reported that AuNPs ameliorated the reduction of megalin-mediated albumin endocytosis in PTECs observed in subAKI, preventing tubular proteinuria and albuminuria. Considering that both glomerular and tubular structures and functions were characterized in animals with subAKI, it is plausible to suggest that these findings may result from the direct effect of AuNPs on PTECs. This hypothesis is strengthened by the observation that AuNPs avoided the inhibition of albumin uptake in LLC-PK1 cells with a higher albumin concentration (mimicking subAKI conditions).

Our results show that naked AuNPs could be a promising tool for the treatment of tubulopathies. Their effects are mediated by shifting the pro-inflammatory response to an anti-inflammatory response. In addition, naked AuNPs present an important anti-proteinuric effect correlated with changes in megalin-mediated PT protein reabsorption. It has been proposed that megalin works as a sensor in the development of tubule-interstitial injury [44,69,70]. The decrease in the expression of megalin has been associated with the development of pro-inflammatory and pro-fibrotic phenotypes [7,8,69,70]. Therefore, by showing that AuNPs prevented the decrease in megalin expression in animals with subAKI, we propose that the beneficial effects of AuNPs on tubule-interstitial injury might be mediated, at least partially, by their capacity to avoid changes in megalin expression, a receptor-mediated endocytosis.

CRediT authorship contribution statement

Rodrigo A.S. Peres: Conceptualization, Methodology, Validation, Formal analysis, Investigation, Data curation, Writing – original draft, Writing – review & editing, Visualization. **Rodrigo P. Silva-Aguiar:** Methodology, Validation, Formal analysis, Investigation, Data curation, Writing – review & editing, Visualization. **Douglas E. Teixeira:** Methodology, Validation, Formal analysis, Investigation, Data curation, Writing – review & editing, Visualization. **Diogo B. Peruchetti:** Methodology, Validation, Formal analysis, Investigation, Data curation, Writing – review & editing, Visualization. **Sarah A.S. Alves:** Investigation, Writing – review & editing, Visualization. **Anna Beatriz C. Leal:** Investigation, Writing – review & editing, Visualization. **Guilherme F. Castro:** Investigation, Writing – review & editing, Visualization. **Natalia B.S. Ribeiro:** Investigation, Writing – review & editing, Visualization. **Fernanda V. Guimarães:** Investigation, Writing – review & editing, Visualization. **Ana Acacia S. Pinheiro:** Conceptualization, Resources, Formal analysis, Writing – review & editing, Visualization, Funding acquisition. **Patrícia M.R. e Silva:** Conceptualization, Resources, Formal analysis, Writing – review & editing, Visualization, Funding acquisition. **Marco A. Martins:** Conceptualization, Resources, Formal analysis, Writing – review & editing, Visualization, Funding acquisition. **Celso Caruso-Neves:** Conceptualization, Methodology, Validation, Formal analysis, Investigation, Resources, Data curation, Writing – original draft, Writing – review & editing, Visualization, Supervision, Project administration, Funding acquisition.

Declaration of Competing Interest

The authors declare that they have no known competing financial interests or personal relationships that could have appeared to influence the work reported in this paper.

Data availability

Data will be made available on request.

References

[1] P. Romagnani, G. Remuzzi, R. Glassock, A. Levin, K.J. Jager, M. Tonelli, Z. Massy, C. Wanner, H.J. Anders, Chronic kidney disease, Nat. Rev. Dis. Primers. 3 (2017) 17088, https://doi.org/10.1038/nrdp.2017.88.

[2] GBD Chronic Kidney Disease Collaboration, Global, regional, and national burden of chronic kidney disease, 1990-2017: a systematic analysis for the global burden of Disease study 2017, Lancet 395 (2020) 709–733, https://doi.org/10.1016/S0140-6736(20)30045-3.

[3] J.A. Kellum, P. Romagnani, G. Ashuntantang, C. Ronco, A. Zarbock, H.J. Anders, Acute kidney injury, Nat. Rev. Dis. Primers 7 (2021) 52, https://doi.org/10.1038/s41572-021-00284-z.

[4] Kidney Disease: Improving Global Outcomes (KDIGO) Acute Kidney Injury Work Group, KDIGO clinical practice guideline for acute kidney injury, Kidney Int. Suppl. 2 (2012) 1–138, https://doi.org/10.1038/kisup.2012.1.

[5] M. Haase, J.A. Kellum, C. Ronco, Subclinical AKI–an emerging syndrome with important consequences, Nat. Rev. Nephrol. 8 (2012) 735–739, https://doi.org/10.1038/nrneph.2012.197.

[6] J. Vanmassenhove, W. Van Biesen, R. Vanholder, N. Lameire, Subclinical AKI: ready for primetime in clinical practice? J. Nephrol. 32 (2019) 9–16, https://doi.org/10.1007/s40620-018-00566-y.

[7] D.E. Teixeira, D.B. Peruchetti, L.S. Silva, R.P. Silva-Aguiar, M.B. Oquendo, J. L. Silva-Filho, C.M. Takiya, J.H. Leal-Cardoso, A.A.S. Pinheiro, C. Caruso-Neves, Lithium ameliorates tubule-interstitial injury through activation of the mTORC2/protein kinase B pathway, PLoS One 14 (2019), e0215871, https://doi.org/10.1371/journal.pone.0215871.

[8] D.B. Peruchetti, J.L. Silva-Filho, R.P. Silva-Aguiar, D.E. Teixeira, C.M. Takiya, M. C. Souza, M.D.G. Henriques, A.A.S. Pinheiro, C. Caruso-Neves, IL-4 receptor α chain protects the kidney against tubule-interstitial injury induced by albumin overload, Front. Physiol. 11 (2020) 172, https://doi.org/10.3389/fphys.2020.00172.

[9] D.B. Peruchetti, P.F.R. Barahuna-Filho, R.P. Silva-Aguiar, T.P. Abreu, C.M. Takiya, J. Cheng, A.A.S. Pinheiro, L. Cebotaru, W.B. Guggino, C. Caruso-Neves, Megalin-mediated albumin endocytosis in renal proximal tubules is involved in the antiproteinuric effect of angiotensin II type 1 receptor blocker in a subclinical acute kidney injury animal model, Biochim. Biophys. Acta Gen. Subj. 1865 (2021), 129950, https://doi.org/10.1016/j.bbagen.2021.129950.

[10] F. Fang, X. Hu, X. Dai, S. Wang, Z. Bai, J. Chen, J. Pan, X. Li, J. Wang, Y. Li, Subclinical acute kidney injury is associated with adverse outcomes in critically ill neonates and children, Crit. Care 22 (2018) 256, https://doi.org/10.1186/s13054-018-2193-8.

[11] W.F. Kean, I.R. Kean, Clinical pharmacology of gold, Inflammopharmacology 16 (3) (2008) 112–125, https://doi.org/10.1007/s10787-007-0021-x.

[12] T.T. Antonovych, Gold nephropathy, Ann. Clin. Lab. Sci. 11 (5) (1981) 386–391.

[13] E.S. Glazer, C. Zhu, A.N. Hamir, A. Borne, C.S. Thompson, S.A. Curley, Biodistribution and acute toxicity of naked gold nanoparticles in a rabbit hepatic tumor model, Nanotoxicology 5 (4) (2011) 459–468, https://doi.org/10.3109/17435390.2010.516026.

[14] F.K. Alanazi, A.A. Radwan, I.A. Alsarra, Biopharmaceutical applications of nanogold, Saudi Pharm. J. 18 (4) (2010) 179–193, https://doi.org/10.1016/j.jsps.2010.07.002.

[15] X. Xiang, S. Feng, J. Chen, J. Feng, Y. Hou, Y. Ruan, X. Weng, G. Milcovich, Gold nanoparticles/electrochemically expanded graphite composite: a bifunctional platform toward glucose sensing and SERS applications, J. Electroanal. Chem. 851 (2019), 113471, https://doi.org/10.1016/j.jelechem.2019.113471.

[16] Y.C. Yeh, B. Creran, V.M. Rotello, Gold nanoparticles: preparation, properties, and applications in bionanotechnology, Nanoscale 4 (6) (2012) 1871–1880, https://doi.org/10.1039/c1nr11188d.

[17] R. Herizchi, E. Abbasi, M. Milani, A. Akbarzadeh, Current methods for synthesis of gold nanoparticles, Artif. Cells Nanomed. Biotechnol. 44 (2) (2016) 596–602, https://doi.org/10.3109/21691401.2014.971807.

[18] J.P. Almeida, E.R. Figueroa, R.A. Drezek, Gold nanoparticle mediated cancer immunotherapy, Nanomedicine 10 (3) (2014) 503–514, https://doi.org/10.1016/j.nano.2013.09.011.

[19] H. Lee, M.Y. Lee, S.H. Bhang, B.S. Kim, Y.S. Kim, J.H. Ju, K.S. Kim, S.K. Hahn, Hyaluronate-gold nanoparticle/tocilizumab complex for the treatment of rheumatoid arthritis, ACS Nano 8 (5) (2014) 4790–4798, https://doi.org/10.1021/nn500685h.

[20] S.M. Lee, H.J. Kim, Y.J. Ha, Y.N. Park, S.K. Lee, Y.B. Park, K.H. Yoo, Targeted chemo-photothermal treatments of rheumatoid arthritis using gold half-shell multifunctional nanoparticles, ACS Nano 7 (1) (2013) 50–57, https://doi.org/10.1021/nn301215q.

[21] C.Y. Tsai, A.L. Shiau, S.Y. Chen, Y.H. Chen, P.C. Cheng, M.Y. Chang, D.H. Chen, C. H. Chou, C.R. Wang, C.L. Wu, Amelioration of collagen-induced arthritis in rats by nanogold, Arthritis Rheum. 56 (2) (2007) 544–554, https://doi.org/10.1002/art.22401.

[22] D. Di Bella, J.P.S. Ferreira, R.N.O. Silva, C. Echem, A. Milan, E.H. Akamine, M. H. Carvalho, S.F. Rodrigues, Gold nanoparticles reduce inflammation in cerebral microvessels of mice with sepsis, J. Nanobiotechnology. 19 (1) (2021) 52, https://doi.org/10.1186/s12951-021-00796-6.

[23] E. Barreto, M.F. Serra, R.V. Dos Santos, C.E. Dos Santos, J. Hickmann, A.C. Cotias, C.R. Pão, N. Trindade, V. Schimidt, C. Giacomelli, V.F. Carvalho, P.M. Rodrigues E. Silva, R.S. Cordeiro, M.A. Martins, Local administration of gold nanoparticles prevents pivotal pathological changes in murine models of atopic asthma, J. Biomed. Nanotechnol. 11 (6) (2015) 1038–1050, https://doi.org/10.1166/jbn.2015.2024.

[24] M.F. Serra, A.C. Cotias, A.S. Pimentel, A.C.S. Arantes, A.L.A. Pires, M. Lanzetti, J. M. Hickmann, E. Barreto, V.F. Carvalho, P.M.R.E. Silva, R.S.B. Cordeiro, M. A. Martins, Gold nanoparticles inhibit steroid-insensitive asthma in mice preserving histone deacetylase 2 and NRF2 pathways, Antioxidants 11 (9) (2022) 1659, https://doi.org/10.3390/antiox11091659.

[25] C.H. Choi, J.E. Zuckerman, P. Webster, M.E. Davis, Targeting kidney mesangium by nanoparticles of defined size, Proc. Natl. Acad. Sci. U. S. A. 108 (2011) 656–661, https://doi.org/10.1073/pnas.1103573108.

[26] C. Zhou, M. Long, Y. Qin, X. Sun, J. Zheng, Luminescent gold nanoparticles with efficient renal clearance, Angew. Chem. Int. Ed. Eng. 50 (2011) 3168–3172, https://doi.org/10.1002/anie.201007321.

[27] Y. Ma, F. Cai, Y. Li, J. Chen, F. Han, W. Lin, A review of the application of nanoparticles in the diagnosis and treatment of chronic kidney disease, Bioact. Mater. 5 (2020) 732–743, https://doi.org/10.1016/j.bioactmat.2020.05.002.

[28] M.G. Lawrence, M.K. Altenburg, R. Sanford, J.D. Willett, B. Bleasdale, B. Ballou, J. Wilder, F. Li, J.H. Miner, U.B. Berg, O. Smithies, Permeation of macromolecules into the renal glomerular basement membrane and capture by the tubules, Proc. Natl. Acad. Sci. U. S. A. 114 (2017) 2958–2963, https://doi.org/10.1073/pnas.1616457114.

[29] M.A. Khan, M.J. Khan, Nano-gold displayed anti-inflammatory property via NF-kB pathways by suppressing COX-2 activity, Artif Cells Nanomed Biotechnol. 46 (2018) 1149–1158, https://doi.org/10.1080/21691401.2018.1446968.

[30] M.A. Dkhil, M.F. Khalil, A.A. Bauomy, S. Diab, Al-Quraishy, Efficacy of gold nanoparticles against nephrotoxicity induced by schistosoma mansoni infection in mice, Biomed. Environ. Sci. 29 (2016) 773–781, https://doi.org/10.3967/bes2016.104.

[31] K. Manna, S. Mishra, M. Saha, S. Mahapatra, C. Saha, G. Yenge, N. Gaikwad, R. Pal, D. Oulkar, K. Banerjee, K. Das Saha, Amelioration of diabetic nephropathy using pomegranate peel extract-stabilized gold nanoparticles: assessment of NF-κB and Nrf2 signaling system, Int. J. Nanomedicine 14 (2019) 1753–1777, https://doi.org/10.2147/IJN.S176013.

[32] G. Alomari, B. Al-Trad, S. Hamdan, A. Aljabali, M. Al-Zoubi, N. Bataineh, J. Qar, M. M. Tambuwala, Gold nanoparticles attenuate albuminuria by inhibiting podocyte injury in a rat model of diabetic nephropathy, Drug Deliv Transl. Res. 10 (2020) 216–226, https://doi.org/10.1007/s13346-019-00675-6.

[33] C.D. De Souza, B.R. Nogueira, M.E.C.M. Rostelato, Review of the methodologies used in the synthesis gold nanoparticles by chemical reduction, J. Alloys Compd. 798 (2019) 714–740, https://doi.org/10.1016/j.jallcom.2019.05.153.

[34] V.G. Portella, J.L. Silva-Filho, S.S. Landgraf, T.B. de Rico, M.A. Vieira, C.M. Takiya, M.C. Souza, M.G. Henriques, C. Canetti, A.A. Pinheiro, C.F. Benjamim, C. Caruso-Neves, Sepsis-surviving mice are more susceptible to a secondary kidney insult, Crit. Care Med. 41 (2013) 1056–1068, https://doi.org/10.1097/CCM.0b013e3182746696.

[35] S.S. Landgraf, L.S. Silva, D.B. Peruchetti, G.M. Sirtoli, F. Moraes-Santos, V. G. Portella, J.L. Silva-Filho, C.S. Pinheiro, T.P. Abreu, C.M. Takiya, C.F. Benjamin, A.A. Pinheiro, C. Canetti, C. Caruso-Neves, 5-Lypoxygenase products are involved in renal tubulointerstitial injury induced by albumin overload in proximal tubules in mice, PLoS One 9 (2014), e107549, https://doi.org/10.1371/journal.pone.0107549.

[36] R.P. Silva-Aguiar, N.C.F. Bezerra, M.C. Lucena, G.M. Sirtoli, R.T. Sudo, G. Zapata-Sudo, C.M. Takiya, A.A.S. Pinheiro, W.B. Dias, C. Caruso-Neves, O-GlcNAcylation reduces proximal tubule protein reabsorption and promotes proteinuria in spontaneously hypertensive rats, J. Biol. Chem. 293 (2018) 12749–12758, https://doi.org/10.1074/jbc.RA118.001746.

[37] C.D. Schuh, M. Polesel, E. Platonova, D. Haenni, A. Gassama, N. Tokonami, S. Ghazi, M. Bugarski, O. Devuyst, U. Ziegler, A.M. Hall, Combined structural and functional imaging of the kidney reveals major axial differences in proximal tubule endocytosis, J. Am. Soc. Nephrol. 29 (2018) 2696–2712, https://doi.org/10.1681/ASN.2018050522.

[38] D.E. Teixeira, D.B. Peruchetti, M.C. Souza, M.G. Das Graças Henriques, A.A. S. Pinheiro, C. Caruso-Neves, A high salt diet induces tubular damage associated with a pro-inflammatory and pro-fibrotic response in a hypertension-independent manner, Biochim. Biophys. Acta Mol. basis Dis. 1866 (2020), 165907, https://doi.org/10.1016/j.bbadis.2020.165907.

[39] R.N. Hull, W.R. Cherry, G.W. Weaver, The origin and characteristics of a pig kidney cell strain, LLC-PK, In Vitro 12 (1976) 670–677, https://doi.org/10.1007/BF02797469.

[40] Y. Takakura, T. Morita, M. Fujikawa, M. Hayashi, H. Sezaki, M. Hashida, R. T. Borchardt, Characterization of LLC-PK1 kidney epithelial cells as an in vitro model for studying renal tubular reabsorption of protein drugs, Pharm. Res. 12 (1995) 1968–1972, https://doi.org/10.1023/a:1016256325921.

[41] R. Nielsen, H. Birn, S.K. Moestrup, M. Nielsen, P. Verroust, E.I. Christensen, Characterization of a kidney proximal tubule cell line, LLC-PK1, expressing endocytotic active megalin, J. Am. Soc. Nephrol. 9 (1998) 1767–1776, https://doi.org/10.1681/ASN.V9101767.

[42] D.B. Peruchetti, R.P. Silva-Aguiar, G.M. Siqueira, W.B. Dias, C. Caruso-Neves, High glucose reduces megalin-mediated albumin endocytosis in renal proximal tubule cells through protein kinase B O-GlcNAcylation, J. Biol. Chem. 293 (2018) 11388–11400, https://doi.org/10.1074/jbc.RA117.001337.

[43] R.P. Silva-Aguiar, D.B. Peruchetti, L.S. Florentino, C.M. Takiya, M.P. Marzolo, W. B. Dias, A.A.S. Pinheiro, C. Caruso-Neves, Albumin expands albumin reabsorption capacity in proximal tubule epithelial cells through a positive feedback loop between AKT and megalin, Int. J. Mol. Sci. 23 (2022) 848, https://doi.org/10.3390/ijms23020848.

[44] C. Caruso-Neves, A.A. Pinheiro, H. Cai, J. Souza-Menezes, W.B. Guggino, PKB and megalin determine the survival or death of renal proximal tubule cells, Proc. Natl.

Acad. Sci. U. S. A. 103 (2006) 18810–18815, https://doi.org/10.1073/pnas.0605029103.

[45] D.B. Peruchetti, A.C. Freitas, V.C. Pereira, J.V. Lopes, C.M. Takiya, N.R. F. Nascimento, A.A.S. Pinheiro, C. Caruso-Neves, PKB is a central molecule in the modulation of Na+-ATPase activity by albumin in renal proximal tubule cells, Arch. Biochem. Biophys. 674 (2019), 108115, https://doi.org/10.1016/j.abb.2019.108115.

[46] K.R. Long, Y. Rbaibi, M.L. Gliozzi, Q. Ren, O.A. Weisz, Differential kidney proximal tubule cell responses to protein overload by albumin and its ligands, Am. J. Physiol. Ren. Physiol. 318 (2020) F851–F859, https://doi.org/10.1152/ajprenal.00490.2019.

[47] R. Nielsen, E.I. Christensen, H. Birn, Megalin and cubilin in proximal tubule protein reabsorption: from experimental models to human disease, Kidney Int. 89 (2016) 58–67, https://doi.org/10.1016/j.kint.2015.11.007.

[48] A. Levin, M. Tonelli, J. Bonventre, J. Coresh, J.A. Donner, A.B. Fogo, C.S. Fox, R. T. Gansevoort, H.J.L. Heerspink, M. Jardine, B. Kasiske, A. Köttgen, M. Kretzler, A. S. Levey, V.A. Luyckx, R. Mehta, O. Moe, G. Obrador, N. Pannu, C.R. Parikh, V. Perkovic, C. Pollock, P. Stenvinkel, K.R. Tuttle, D.C. Wheeler, K.U. Eckardt, ISN global kidney health summit participants, global kidney health 2017 and beyond: a roadmap for closing gaps in care, research, and policy, Lancet 390 (2017) 1888–1917, https://doi.org/10.1016/S0140-6736(17)30788-2.

[49] M.G. Shlipak, S.L. Tummalapalli, L.E. Boulware, M.E. Grams, J.H. Ix, V. Jha, A. P. Kengne, M. Madero, B. Mihaylova, N. Tangri, M. Cheung, M. Jadoul, W. C. Winkelmayer, S. Zoungas, Conference participants, the case for early identification and intervention of chronic kidney disease: conclusions from a kidney Disease: improving global outcomes (KDIGO) controversies conference, Kidney Int. 99 (2021) 34–47, https://doi.org/10.1016/j.kint.2020.10.012.

[50] C. Villiers, H. Freitas, R. Couderc, M.B. Villiers, P. Marche, Analysis of the toxicity of gold nano particles on the immune system: effect on dendritic cell functions, J. Nanopart. Res. 12 (2010) 55–60, https://doi.org/10.1007/s11051-009-9692-0.

[51] S. Soares, J. Sousa, A. Pais, C. Vitorino, Nanomedicine: principles, properties, and regulatory issues, Front. Chem. 6 (2018) 360, https://doi.org/10.3389/fchem.2018.00360.

[52] Y. Pan, S. Neuss, A. Leifert, M. Fischler, F. Wen, U. Simon, G. Schmid, W. Brandau, W. Jahnen-Dechent, Size-dependent cytotoxicity of gold nanoparticles, Small 3 (2007) 1941–1949, https://doi.org/10.1002/smll.200700378.

[53] W.H. De Jong, W.I. Hagens, P. Krystek, M.C. Burger, A.J. Sips, R.E. Geertsma, Particle size-dependent organ distribution of gold nanoparticles after intravenous administration, Biomaterials 29 (2008) 1912–1919, https://doi.org/10.1016/j.biomaterials.2007.12.037.

[54] Y.S. Chen, Y.C. Hung, I. Liau, G.S. Huang, Assessment of the in vivo toxicity of gold nanoparticles, Nanoscale Res. Lett. 4 (2009) 858–864, https://doi.org/10.1007/s11051-009-9334-6.

[55] G.K. Ferreira, E. Cardoso, F.S. Vuolo, M. Michels, E.T. Zanoni, M. Carvalho-Silva, L. M. Gomes, F. Dal-Pizzol, G.T. Rezin, E.L. Streck, M.M. Paula, Gold nanoparticles alter parameters of oxidative stress and energy metabolism in organs of adult rats, Biochem. Cell Biol. 93 (2015) 548–557, https://doi.org/10.1139/bcb-2015-0030.

[56] C. Lopez-Chaves, J. Soto-Alvaredo, M. Montes-Bayon, J. Bettmer, J. Llopis, C. Sanchez-Gonzalez, Gold nanoparticles: distribution, bioaccumulation and toxicity. In vitro and in vivo studies, Nanomedicine 14 (2018) 1–12, https://doi.org/10.1016/j.nano.2017.08.011.

[57] K. Isoda, A. Tanaka, C. Fuzimori, M. Echigoya, Y. Taira, I. Taira, Y. Shimizu, Y. Akimoto, H. Kawakami, I. Ishida, Toxicity of gold nanoparticles in mice due to nanoparticle/drug interaction induces acute kidney damage, Nanoscale Res. Lett. 15 (2020) 141, https://doi.org/10.1186/s11671-020-03371-4.

[58] N.S. Al-Harbi, S.T. Alrashood, N.J. Siddiqi, M.M. Arafah, A. Ekhzaimy, H.A. Khan, Effect of naked and PEG-coated gold nanoparticles on histopathology and cytokines expression in rat liver and kidneys, Nanomedicine (London) 15 (2020) 289–302, https://doi.org/10.2217/nnm-2019-0220.

[59] Z. He, C. Li, X. Zhang, R. Zhong, H. Wang, J. Liu, L. Du, The effects of gold nanoparticles on the human blood function, Artif. Cells Nanomed Biotechnol. 46 (2018) 720–726, https://doi.org/10.1080/21691401.2018.1468769.

[60] A.V. Aseichev, O.A. Azizova, E.M. Beckman, O.I. Skotnikova, L.B. Dudnik, O. N. Shcheglovitova, V.I. Sergienko, Effects of gold nanoparticles on erythrocyte hemolysis, Bull. Exp. Biol. Med. 156 (2014) 495–498, https://doi.org/10.1007/s10517-014-2383-6.

[61] L.A. Dykman, N.G. Khlebtsov, Immunological properties of gold nanoparticles, Chem. Sci. 8 (2017) 1719–1735, https://doi.org/10.1039/c6sc03631g.

[62] Y. Liu, J. Hardie, X. Zhang, V.M. Rotello, Effects of engineered nanoparticles on the innate immune system, Semin. Immunol. 34 (2017) 25–32, https://doi.org/10.1016/j.smim.2017.09.011.

[63] S. Tomić, J. Đokić, S. Vasilijić, N. Ogrinc, R. Rudolf, P. Pelicon, D. Vučević, P. Milosavljević, S. Janković, I. Anžel, J. Rajković, M.S. Rupnik, B. Friedrich, M. Colić, Size-dependent effects of gold nanoparticles uptake on maturation and antitumor functions of human dendritic cells in vitro, PLoS One 9 (2014), e96584, https://doi.org/10.1371/journal.pone.0096584.

[64] S. Michelini, F. Barbero, A. Prinelli, P. Steiner, R. Weiss, T. Verwanger, A. Andosch, U. Lütz-Meindl, V.F. Puntes, D. Drobne, A. Duschl, J. Horejs-Hoeck, Gold nanoparticles (AuNPs) impair LPS-driven immune responses by promoting a tolerogenic-like dendritic cell phenotype with altered endosomal structures, Nanoscale 13 (2021) 7648–7666, https://doi.org/10.1039/d0nr09153g.

[65] H. Rizwan, J. Mohanta, S. Si, A. Pal, Gold nanoparticles reduce high glucose-induced oxidative-nitrosative stress regulated inflammation and apoptosis via tuberin-mTOR/NF-κB pathways in macrophages, Int. J. Nanomedicine 12 (2017) 5841–5862, https://doi.org/10.2147/IJN.S141839.

[66] L.E.M. Heeb, C. Egholm, O. Boyman, Evolution and function of interleukin-4 receptor signaling in adaptive immunity and neutrophils, Genes Immun. 21 (2020) 143–149, https://doi.org/10.1038/s41435-020-0095-7.

[67] R.F. Jr Lemanske, W.W. Busse, Asthma: clinical expression and molecular mechanisms, J. Allergy Clin. Immunol. 125 (2010) S95–102, https://doi.org/10.1016/j.jaci.2009.10.047.

[68] K.H. Shalaby, J.G. Martin, Overview of asthma; the place of the T cell, Curr. Opin. Pharmacol. 10 (2010) 218–225, https://doi.org/10.1016/j.coph.2010.03.004.

[69] D. Liu, Y. Wen, T.T. Tang, L.L. Lv, R.N. Tang, H. Liu, K.L. Ma, S.D. Crowley, B. C. Liu, Megalin/cubulin-lysosome-mediated albumin reabsorption is involved in the tubular cell activation of NLRP3 inflammasome and tubulointerstitial inflammation, J. Biol. Chem. 290 (2015) 18018–18028, https://doi.org/10.1074/jbc.M115.662064.

[70] J.R. Charlton, W. Tan, G. Daouk, L. Teot, S. Rosen, K.M. Bennett, A. Cwiek, S. Nam, F. Emma, F. Jouret, J.P. Oliveira, L. Tranebjærg, C. Frykholm, S. Mane, F. Hildebrandt, T. Srivastava, T. Storm, E.I. Christensen, R. Nielsen, Beyond the tubule: pathological variants of LRP2, encoding the megalin receptor, result in glomerular loss and early progressive chronic kidney disease, Am. J. Physiol. Ren. Physiol. 319 (2020) F988–F999, https://doi.org/10.1152/ajprenal.00295.2020.